applied sciences

MDPI

Article

Smart Wireless CO_2 Sensor Node for IoT Based Strategic Monitoring Tool of The Risk of The Indoor SARS-CoV-2 Airborne Transmission

C. Bambang Dwi Kuncoro [1,*], Aurelia Amaris [2] and Arvanida Feizal Permana [1]

[1] Department of Refrigeration, Air Conditioning, and Energy Engineering, National Chin-Yi University of Technology, Taichung 41170, Taiwan
[2] Department of Informatics Engineering, Faculty of Computer Science, Universitas Brawijaya, Malang, Jawa Timur 65145, Indonesia
* Correspondence: bkuncoro@ncut.edu.tw; Tel.: +886-4-239-24505 (ext. 8274)

Abstract: A close correlation between CO_2 concentration and aerosol enables the wide utilization of CO_2 concentration as a good representation of Severe Acute Respiratory Syndrome-Coronavirus-2 infection airborne transmission. On the other side, many indoor air-quality monitoring devices have been developed for indoor monitoring applications. However, most of them are multiparameter air-quality sensor systems and tend to consume relatively high power, are relatively large devices, and are fairly expensive; therefore, they not meet the requirement for indoor monitoring applications. This paper presents a smart wireless sensor node that can measure and monitor CO_2 concentration levels. The node was designed to meet the requirements of indoor air-quality monitoring applications by considering several factors, such as compact size, low cost, and low power, as well as providing real-time, continuous, reliable, and remote measurement. Furthermore, the commercial off-the-shelf and low-power consumption components are chosen to fit with the low-cost development and reduce energy consumption. Moreover, a low-power algorithm and cloud-based data logger also were applied to minimize the total power consumption. This power strategy was applied as a preliminary development toward an autonomous sensor node. The node has a compact size and consumes low energy for one cycle of CO_2 measurement, accompanied by high accuracy with very low measurement error. The experiment result revealed the node could measure and monitor in real-time continuous, reliable, and remote CO_2 concentration levels in indoor and outdoor environments. A user interface visualizes CO_2 concentration graphically and numerically using the Adafruit platform for easy accessibility over the Internet of Things. The developed node is very promising and suitable for indoor CO_2 monitoring applications with the acquired data that could be utilized as an indicator to minimize the risk of indoor Severe Acute Respiratory Syndrome-Coronavirus-2 airborne transmission.

Keywords: sensor node; low-power; COVID-19; monitoring; Internet of Things

check for updates

Citation: Kuncoro, C.B.D.; Amaris, A.; Permana, A.F. Smart Wireless CO_2 Sensor Node for IoT Based Strategic Monitoring Tool of The Risk of The Indoor SARS-CoV-2 Airborne Transmission. *Appl. Sci.* **2022**, *12*, 10784. https://doi.org/10.3390/app122110784

Academic Editors: Ryan Gibson and Hadi Larijani

Received: 2 October 2022
Accepted: 21 October 2022
Published: 25 October 2022

1. Introduction

Indoor air quality (IAQ) has a significant role in enhancing the indoor environment quality of room occupants as a factor influencing health, comfort, performance, concentration, and safety [1–3]. Several studies have revealed that indoor environments have major air pollutants higher than outdoor environments [4–6]. Therefore, the impacts have become worse because most people spend an average of 80–90% of their daily time indoors, and air pollutants expose them more than outdoor air pollutants [7,8]. Based on the high potential for worse health effects, IAQ monitoring is observed as a crucial issue for indoor occupants regarding the guarantee of human health and well-being, especially during the Corona Virus Disease-19 (COVID-19) pandemic. Although the health protocols released by the World Health Organization (WHO), such as wearing a mask, cleaning the hands, and maintaining social distance, are effective for protecting from Severe Acute Respiratory

Syndrome-Coronavirus-2 (SARS-CoV-2) infection, the monitoring IAQ is still a significant key to minimize the risk of SARS-CoV-2 airborne transmission [9]. Furthermore, the level of Carbon dioxide (CO_2) concertation receives primary attention of IAQ monitoring systems today. Therefore, in many HVAC (Heating, Ventilation, and Air-Conditioning) systems, control of the fresh airflow rate mostly uses indoor CO_2 concentration as the indicator [10]. Moreover, the purpose of indoor CO_2 concentration measurement and monitoring is crucial, not only for CO_2 exposure effects evaluation but also for the study of airborne transmission of various contagious diseases, e.g., tuberculosis, measles, influenza, H1N1, and coronavirus (COVID-19). In other words, an indication of indoor airborne cross-infection risk can be evaluated based on the indoor CO_2 concentration level [11–13].

Multiple studies have demonstrated the SARS-CoV-2 virus's airborne transmission mainly through particles from respiratory inhalation that contains the virus [14–16]. The particles spread out during lung-related activities such as breathing, laughing, speaking, singing, etc. The particles are distinguished into two sizes that are droplets with large sizes and aerosols with small sizes. When larger particles spread in the air, they quickly drop to the ground, while smaller particles easily float and spread in enclosed spaces for a longer period [17]. Because CO_2 concentration has a close correlation with aerosol particles, the immediate CO_2 concentration can be utilized as a proper representative for the concentration of aerosol particles, assuming no other substantial CO_2 source exists in the air [11,18,19]. Other studies confirmed that the exhaled air from inhalation contains aerosols and also has the potential to bring the SARS-CoV-2 virus where the infected particles floating in the air could be detected for up to 3 h [20,21]. The risk of airborne transmission of the SARS-CoV-2 virus also occurs significantly in an indoor environment with poor ventilation or without a ventilation system. Therefore, it is critical to keep the concentration of aerosol particles as low as possible to reduce the danger of SARS-CoV-2 virus infection, especially during the COVID-19 pandemic, as presented in an aerosol infection model in [22]. Moreover, the authors in [11] presented that indoor CO_2 concentration is a good indicator for SARS-CoV-2 transmission risk and can be examined easily and immediately using an IAQ sensor. The sensor measurement results are useful for indoor CO_2 monitoring and SARS-CoV-2 transmission risk assessment where several room occupants spend their daily time indoors. The risk indicator is evaluated based on the volume mixing ratio of the excess CO_2 inhaled by uninfected people in an environment for 1 h.

Several studies have developed a sensor system for monitoring the concentration levels of indoor CO_2. In [23], a sensor node was developed to monitor air quality remotely in a subway station. The design focused on the size, cost, and reliability aspects. The node uses a Non-Dispersive Infrared (NDIR)-based CO_2 sensor for CO_2 sensing and Sensorion Humidity Temperature (SHT)75 sensor for temperature and humidity sensing. It utilizes ATmega 128L as a processor and Chipcon CC2420 as a wireless communication modem. A 12 V external power supply is applied as power source. The sensor node was applied in a real subway station using a Wireless Sensor Network (WSN) system, with the measuring error rate of the CO_2 sensor being $\pm$ 30 ppm. The authors in [24] developed an air-quality monitoring system for the apartment's data collection and analytics. They used an IoT system and a mechanical exhaust system to control air quality due to the occupants' schedule, behavior, and personal preferences. This research showed the possibility of integration of sensor data in a cloud system and solved the sensor network cost. In [25], a sensor node was developed and equipped with multiple sensors, a CO_2 (MG811) sensor, a temperature and humidity (RTH03) sensor, and a VOC (TGS2602) sensor, to monitor indoor air quality. The node utilizes an Arduino Uno microcontroller board and the Digi XBee module with the radio networking protocol of IEEE 802.15.4 as a communication device. The module can be operated as either coordinator, router or end device. The sensor node can measure CO_2 levels in indoor areas at around $\pm$500 ppm. The authors in [26] introduced an environment-monitoring system based on the IoT. It was used to monitor indoor air quality in the educational facility for a healthy learning environment. The system was built using a ThunderBoard Sense 2 wireless sensor board with a built-in CO_2 sensor

and other sensors such as TVOC, ultraviolet index, temperature, relative humidity, air pressure, ambient light, and noise level. The sensor node communicates using a BeagleBone Black Wireless (BBBW), which had an ARM Cortex-A8 1GHz to connect with the IoT. Three NiMh AA-size batteries with 3.7 V and 2450 mAh power are the main power source. The power source can support the sensor node for 13 days without battery shortage. The system can monitor environmental parameters in real time and provides feedback to occupants' facilities. During a busy time, the node can detect CO_2 concentrations up to 1200 ppm. The authors in [27] present a wireless gas sensor network for indoor environment-quality monitoring in the school area. The sensor system was built using a Programmable system-on-chip (PSoC) coupled with a Z-Wave module to connect with an internet gateway to transfer the data and combine the data with a comprehensive picture of the whole building. The integrated sensors involve CO_2, temperature, and humidity. The device uses an NDIR CO_2 sensor and an SHT21 sensor to collect CO_2, temperature, and humidity data. The monitoring system is also integrated with the online data platform "EnControl" from Sensing and Control System SL to determine the thermal comfort, ventilation rate, and production rate of CO_2 during a learning activity. A prototype of a CO_2 sensor node was developed for the building's CO_2 measurement and circulation management [28]. The main component of the sensor node includes a COZIR sensor, Arduino Mega for processing, and an NRF24L01 module for communication. Its measurement range is 0–10,000 ppm, with the acquired CO_2 data being transmitted to Rasberry Pi (node sink) using RF communication before subsequent transmission to the server node. An air-quality monitoring system based on IoT was developed in [29]. The system was applied in a university classroom environment to measure O_2, CO, CO_2, and NH_3 concentrations. The ME2-O_2, MQ-7, MG-811, and MQ-135 sensors were used to measure O_2, CO_2, CO, and NH_3, respectively. ATMega32 controls all the sensors to transmit the air-quality data to the web server using an ESP8266 module through WLAN and internet connection in an interval of 5 min. The processed air-quality data were visualized graphically on the web pages and an LCD. The sensor node works using an operating voltage of 5 V and consumes power of 3410 mWh in scheduling mode and 8174 mWh in a full-time mode. A study in [30] presents a compact, low-cost indoor air-quality monitoring system. The platform comprises three sensors, a processor, and a transmission module. The sensors are Si7006 for temperature and relative humidity sensing, CCS811 for CO_2 concentration detection, and PMS7003 for particulate matter measurement. The ATSAMD21G18-48 microcontroller was utilized for data acquisition and processing, and ESP8266-12F was used for wireless data transmission to the MQTT protocol-based cloud server (Grafana platform). The node power source is a 5V external power source using a micro-USB cable. The node is implemented in a two-layer PCB board of 57 mm $\times$ 75 mm.

However, a few single-sensor nodes have been developed for CO_2 concentration measurement that meets indoor application requirements. Most of these sensor systems, as mentioned above, are multiparameter air-quality sensor systems. Moreover, IAQ monitoring devices that are available in the market mentioned in [31–34] also tend to consume relatively high power, are relatively large devices, and are fairly expensive; therefore, they do not meet the requirement for indoor-monitoring applications. The sensor node should have low-power consumption for long-period operation, be easily installed in limited space indoors, and have low-cost development, as well as being easily utilized and accessed.

This paper presents a smart wireless CO_2 sensor node to measure and monitor indoor CO_2 concentration levels. The sensor node is integrated with the IoT system to enable real-time, continuous, reliable, and remote indoor CO_2 measurement and monitoring. Furthermore, the acquired CO_2 concentration level data can be applied as a strategic tool to minimize the risk of the indoor SARS-CoV-2 airborne transmission. A low-power algorithm was applied to drive the sensor node working with low-power consumption toward the autonomous sensor node for long-period operation. The node was designed to meet the requirements of indoor air-quality monitoring applications by considering several factors, such as compact size, low cost, and low power, as well as providing real-time, continuous,

reliable, and remote measurement. Moreover, the sensor node uses the cloud system for data storage that can be accessed using the IoT system. This strategy is not only for enhancing sensor-node accessibility (anywhere and anytime) but also to reduce the total energy consumption of sensor nodes that cannot be met if data storage is applied using a commercial data logger (hardware). With the low-power feature, the developed sensor node has the potential to integrate with a micro energy harvester element, which provides energy for sensor node power storage recharging.

2. Materials and Methods

2.1. Carbon Dioxide (CO_2) Indoor Source and Health Effect

Carbon dioxide gas is a chemical compound characterized as a colorless, odorless, and non-flammable gas. It is released into the air from two sources, namely (1) natural processes, such as organism respiration, organic matter breakdown, gases released from surface waters, forest burning, and volcanic eruptions, and (2) anthropogenic emissions, including industrial activities, burning fossil fuels, and deforestation.

In an indoor environment, human respiration is the main source of CO_2 gas. Therefore, occupant density and ventilation systems are essential factors in determining indoor CO_2 concentrations, although it can also come from household appliances that use fuel burning, such as gas stoves, furnaces, room heaters, and candle burning as well as cigarette smoking [35]. The indoor room has a risk of a high level of CO_2 concentration and can even be higher than the outdoor concentration level. This will occur when the room has poor or no ventilation, or a high density of occupants in a small room. This condition causes the CO_2 released through occupant breathing to accumulate over time and cannot be released outdoors.

CO_2 concentration is commonly applied to evaluate indoor air quality and control of the fresh-air flow rate because its concentration has potential health and performance effects on room occupants. The effects of CO_2 exposure on indoor air quality and human health vary in a wide range of CO_2 concentrations [36]. Table 1 shows the relationship between the concentration of CO_2 exposure and the effect on indoor air quality and human health.

Table 1. Description of CO_2 concentration and indoor air quality.

CO_2 Concentration	350–400 ppm	<600 ppm	1000 ppm	1500 ppm	2000 ppm	>10,000 ppm
Description of indoor air quality with health after effect.	Fresh air and perfect conditions.	Acceptable conditions of IAQ in rooms.	Stuffy and damp air.	Air is perceived as stuffy and not fresh.	People with respiratory illnesses develop a cough, with other weak occupants fainting.	Bad air quality causes increased breathing rates, weakened respiration, headaches, and nausea.

The CO_2 concentration in outdoor environments typically ranges from 350 to 450 ppm. However, the CO_2 concentration will rise if humans are trapped in an enclosed and unventilated room. Unlike other air pollutants, the low concentration of CO_2 gas is safe for human life. However, a high level of CO_2 concentration has various bad effects on humans because it can substitute O_2. At a moderate level, CO_2 concentration causes fatigue, inhibits cognitive functions, and produces headaches. Irrespective of this condition, small elevations from 600 to 1000 ppm also lead to the reduction of cognitive ability and decision-making. The emission of CO_2 is found to subsequently cause sickness or death based on a very high concentration level [37]. Table 2 shows more detail on human physiological and health impacts when exposed to a high level of CO_2 concentration.

Table 2. Physiological and health effects of high CO_2 exposure.

CO_2 Concentration	1000 ppm	2500 ppm	5000 ppm	6% (60 kppm)	7% (70 kppm)	10–15%	17–30%	>30%
Duration	>2.5 h	<2.5 h	>30 min	1–2 min	5 min	1 min	1 min	30 s
Physiological impact/Health effect.	Decision-making abilities and judgment reasoning skills are harmed.	Cognitively marginal or functional disorder.	Headache, lethargy, mental slowness, emotional irritation, and sleep disruption.	Hearing and visual disturbances.	Death	Dizziness, drowsiness, severe muscle twitching, and death.	Loss of controlled activity, coma, convulsions, and death.	Losing consciousness and having seizures (no cerebral functioning).

2.2. SARS-CoV-2 Pathway Transmission

SARS-CoV-2 is an enveloped virus that causes COVID-19. The protein and lipid envelope insulates the genetic material. During infection, the envelope composed of spike proteins has been found to bind with human cells. Similar to other enveloped respiratory viruses, SARS envelopes are unstable and quickly degrade when exposed to surfactants in cleaning solutions and depending on the environmental circumstances [38]. Contact with contaminated objects or surfaces (fomites), direct contact with an infected person, droplet transmission or airborne transmission are all possible ways for humans to become infected with this virus.

The fomite transmission risk of SARS-CoV-2 is considered relatively low compared with direct contact, droplet transmission, and airborne transmission because of many parameters determining the efficiency of environmental transmission. Few cases of COVID-19 have been reported that could be linked to fomite transmission [39,40]. Several studies have investigated the risk of SARS-CoV-2 transmission through virus-laden droplets and airborne pathways. The virus-laden droplets' transmission pathway is large respiratory droplets that spread from an infected person to others at a close distance when the infected person coughs, speaks or sneezes [41,42]. The airborne transmission also contributes significantly to SARS-CoV-2 transmission because small microdroplets may travel in an indoor environment with a distance range up to 10 m from the exhalation of an infected person and can stay afloat in the air for a longer time [15,16]. The illustration of droplets and aerosol transmission is shown in Figure 1.

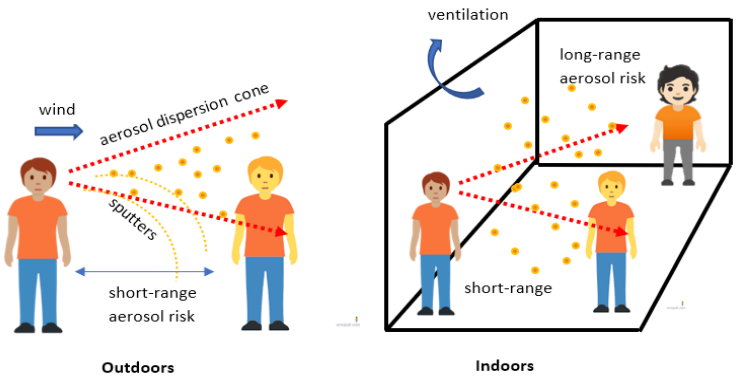

Figure 1. SARS-CoV-2 droplets and airborne transmission in outdoor and indoor environments.

During the breathing process, the exhalation of CO_2 and aerosol is inevitable for humans. In this process, the aerosol concentration was claimed as the pathway of airborne SARS-CoV-2 transmission. Therefore, the concentration of CO_2 can be utilized as a proper proxy for the concentration of aerosol particles. As mentioned in [11–13,18,19], the risk of SARS-CoV-2 transmission has a correlation with the CO_2 concentration level. Especially in an indoor environment, CO_2 concentration levels are usually higher than outdoor

concentrations due to human exhalation. It could be related to increasing the infection risk probability because room occupants commonly inhaled the breath exhaled by one another.

2.3. Proposed CO_2 Sensor Node

2.3.1. Design Overview

The proposed wireless sensor node comprises four units; an air-quality sensor, a processor, a wireless transceiver, and a battery charger, as shown in Figure 2. The CO_2 air-quality sensor is used to sense indoor CO_2 concentration. The main component is a microcontroller to be used for data acquisition and as a main processing unit. The acquired CO_2 data will be recorded and sent to the cloud over an IoT system using a Wi-Fi unit. A rechargeable power storage unit is applied as the main sensor node power source. It stores power from external energy sources (wall adapter power supply, ambient energy) and provides a regulated voltage source to the sensor node through a voltage regulator unit.

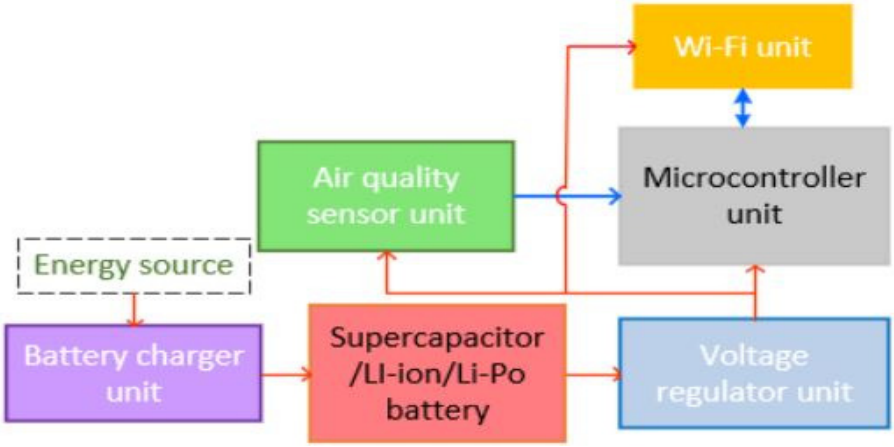

Figure 2. IAQ sensor node architecture.

The sensor node is developed considering the requirements for indoor air-quality monitoring applications. It is designed in a compact size to fit and to be easy to install in limited space. The commercial off-the-shelf (COTS) components available in the market and low-power consumption components are chosen to meet low-cost development and reduce the sensor node's energy consumption, respectively. The low-power mode features are applied using a low-power algorithm to minimize total energy consumption during CO_2 data acquisition and processing. In addition to that, to reduce overall sensor node power consumption, the cloud storage integrated with the IoT system is utilized to store the acquired CO_2 data. During sensor-node active mode (data sensing, processing, transmitting, and logging), the cloud storage system consumes less energy than data storage implemented with a commercial data logger (hardware). With a low-power strategy, the developed sensor node has the potential to integrate with a micro energy harvester as a power source in the further development toward an autonomous CO_2 sensor node. Furthermore, integrating sensor nodes with IoT systems provides indoor CO_2 concentration levels that can be recorded and monitored in real time, are continuous and reliable, and are remote anytime and anywhere. Thus, the indoor CO_2 concentration data will be useful as a strategy tool to minimize the risk of indoor SARS-CoV-2 airborne transmission.

2.3.2. Hardware Design

The sensor- node hardware was designed based on the block diagram in Figure 2. A single board unit composed of sensor-node component circuitry builds a compact device. This development involved the main board and software designs, as well as the components' descriptions as follows.

A. Main Board

Concerning a compact design, all sensor-node components were applied on a double-layer printed circuit board (PCB) with a size of 25 mm × 50 mm. A compact size was appropriately considered for the indoor application requirement, which is easy to install without occupying a large space. Moreover, the developed sensor node will be coupled with an energy harvester module in further development. Therefore, a compact-size sensor node is suitable for this purpose. The sensor node will be installed close to the indoor ambient energy source (artificial light, fan, air conditioning, etc.) to harvest ambient micro energy to prolong the sensor node's main power. This scenario can extend the sensor-node life for a long operation period (autonomous sensor-node system). The PCB layout was designed using Altium Designer software, as shown in Figure 3.

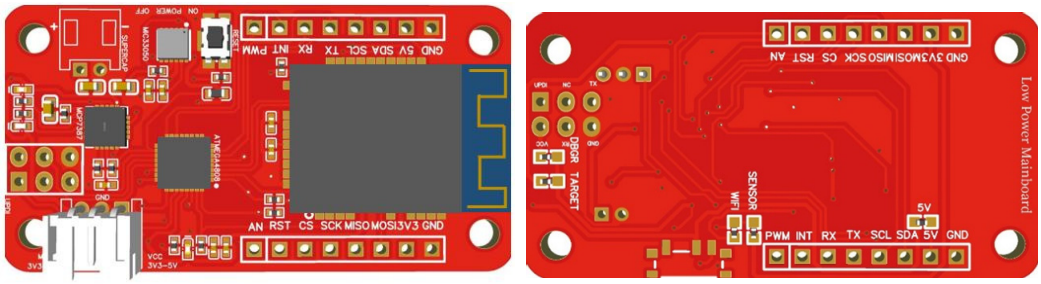

(**a**) (**b**)

Figure 3. PCB design of CO_2 sensor node: (**a**) top layer; (**b**) bottom layer.

The main sensor node components were integrated and soldered on the PCB's top layer, including the microcontroller, Wi-Fi module, and power circuit components. An on-off switch was placed on the PCB's bottom layer. All electronic components integrated to build the sensor node are surface mount devices (SMDs) available in the market, small in size, and consume low power. A CO_2 sensor board was integrated on the top layer side of the sensor node's PCB using a bus connector.

B. Microcontroller

The ATMega4808 was selected to support compact hardware design and low-power consumption features. This microcontroller is a MegaAVR family unit with a low-power architecture [43] with an 8-bit core size, multiple operating frequency up to 20 MHz, a wide range of Flash size up to 48 KB, SRAM size up to 6 KB, and EEPROM size 256 bytes. The module has a wide operating voltage from 1.8 to 5.5 V and provides 3 sleep modes: idle with immediate wake-up functionality, standby, and power-down with limited wake-up functionality. This microcontroller also has a wide range of current consumption that depends on operating frequency; active mode is from 1.2 µA to 11.4 mA, and idle mode is from 1.8 µA to 2.8 mA. In standby mode, it consumes a typical current of 0.7 µA and a maximum current of 16 µA. While in power-down mode, it consumes a typical current of 0.1 µA and a maximum current of 15 µA [44].

The ATMega4808 is easy to purchase at a low cost, which is another criterion for choosing this microcontroller. Several air-quality sensors with common interfaces can also be coupled with this microcontroller using interfaces such as I_2C, SPI, and UART/USART.

C. CO_2 sensor module

The SCD30 sensor module from Sensorion was chosen to sense CO_2 concentration. It offers accurate and stable CO_2 sensing results and is fully calibrated and linearized. The sensor-based NDIR (Non-Dispersive InfraRed) technology has more advantages regarding long-term stability, accuracy, and power consumption rate during CO_2 measurement [45]. The sensor module embedded with SHT31 can measure CO_2, humidity, and temperature. The sensor module has a small package of 35 × 23 × 7 mm^3, as shown in Figure 4. Therefore, it is suitable for the CO_2 sensing front end of the developed sensor node.

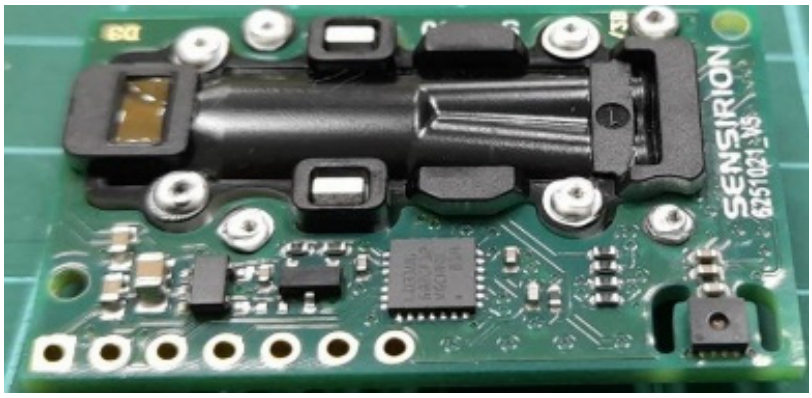

Figure 4. CO_2 sensor module.

The SCD30 sensor module is a calibrated sensor with CO_2 accuracy of ± 30 ppm, a wide detection range of 400–10,000 ppm, and a response time of 20 s. It works in supply voltage ranges from 3.3 to 5.5 V and offers low current consumptions with an average supply current of 19,000 µA and a maximum supply current of 75,000 µA [46]. The measurement output is delivered using I_2C, Modbus, or PWM interfaces

D. Wi-Fi Module

The Wi-Fi module performs sensing-data transmission from the sensor node to the IoT system. Microchip's ATWINC1510 was chosen for this purpose due to its low-power characteristic. It is an IoT network controller based on the IEE 802.11 b/g/n IoT protocol. It can couple with a microcontroller chip to perform low-power IoT networking capability using SPI or UART for the Wi-Fi interface. The ATWINC1510 needs only an external clock source to work in operating frequency ranges from 2.412 to 2.472 MHz using a high-speed crystal or oscillator. The system software can use its 8 MB flash memory. It is equipped with a printed antenna or a micro co-ax (u. FL) connector to achieve a small form-factor design with a dimension of 21.7 × 14.7 × 2.1 mm, as shown in Figure 5.

Figure 5. Wi-Fi module WINC1510.

Microchip's ATWINC1510 is equipped with a switch, power management, Low noise amplifier (LNA), and power amplifier. Considering the low-power requirement, it works at an operating voltage range of 2.7 to 3.6 V, Tx current of 287 mA, Rx current of 83 mA, and power-down mode of 4 µA. In addition, it has an on-chip low-power sleep oscillator and fast host wake-up [47].

E. Power storage

A supercapacitor was selected for the main power storage of the sensor node. The high-power density with fast charge and discharge time was considered to support a low-power sensor node capable of harvesting micro energy from indoor ambient energy and store in energy storage (supercapacitor). Compared with a battery, a supercapacitor has better typical characteristics such as a recharger cycle life of more than 10^6 cycles, self-discharge rate of more than 30%, a wide-range power density of up to 500 W/m^3, faster charging time in the range of sec-min, faster discharging time less than a few min, and usage of the simple charging circuit [48].

The developed sensor node works with an operating voltage of 5 V. A parallel of 2 units 5.5 V 5.0 F was used as power storage for powering up the sensor node with a total capacity of 5.5 V 10 F. The supercapacitor capacity can be increased by enlarging the capacitance of the supercapacitor. The built-in supercapacitor on the developed sensor node was considered to verify the potential of the supercapacitor as power storage for the sensor node that harvests energy from indoor ambient energy. A parallel of 2 units 5.5 V 5.0 F integration is shown in Figure 6.

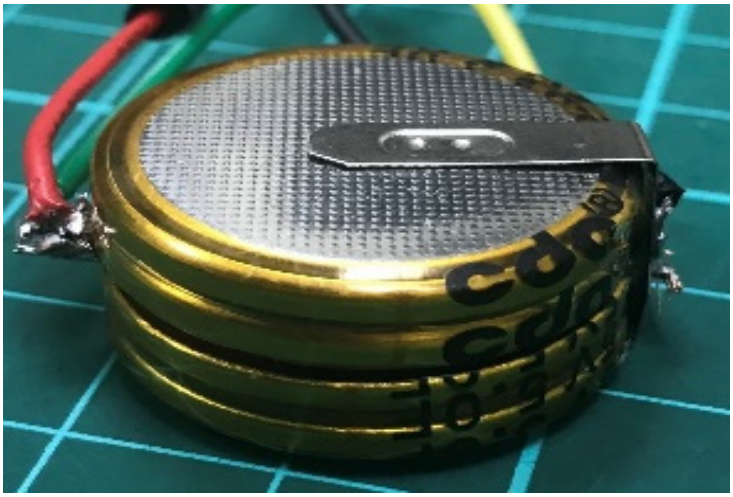

Figure 6. Supercapacitor.

2.3.3. Software Development

The C code-based sensor node software was developed using the Arduino Development Environment (IDE) to control sensor-node operation. The code is composed of two main sections: Setup and Loop. The Setup section is an initialization part that includes variable declaration, I/O setup, and interface setup. The Loop section is divided into the Wi-Fi/internet connection, CO_2 data reading and processing, CO_2 data transmission and logging to the cloud, CO_2 data presentation on the IoT system, and power-down mode. The power-down part puts in between one cycle of CO_2 data measurement. The power-down mode was applied to reduce overall sensor-node power consumption during the CO_2 measurement process. The Adafruit dashboard developed by Adafruit IO was used to visualize CO_2 data and trends on the terminal monitor. It interfaces the recorded CO_2 data in the cloud of the IoT system with a graphical user interface (GUI). The sensor-node program algorithm is presented in a pseudo-code as follows.

3. Result and Discussion

The proposed sensor node was implemented according to the proposed architecture, with the main features being low power and compact size. It was verified with testing, validating, measurement, and a field experiment to ensure the developed device meets the design requirements.

3.1. Device Implementation

The device implementation can be looked at in Figure 7. The sensor node prototype was built with a compact and small board to be suitable for indoor CO_2 measurement. The size of the device is 25 × 60 mm. The main board is composed of a processor, Wi-Fi module, and power circuit located on the bottom of the sensor node, as depicted in Figure 7a. The CO_2 sensor from Sensorion plug-in on the top of the main board, as shown in Figure 7b, includes a parallel of 2 units 5.5 V 5.0 F supercapacitor (Figure 7c). This configuration was considered for further development to integrate the developed sensor node with a micro-energy harvesting module coupled on the bottom of the main board.

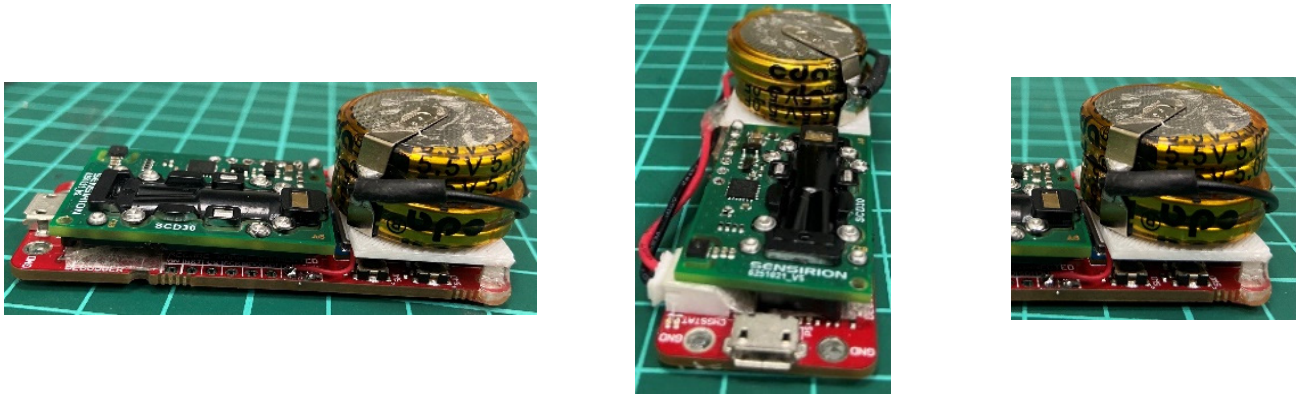

(**a**) (**b**) (**c**)

Figure 7. The CO_2 sensor node prototype: (**a**) side view; (**b**) top view; (**c**) supercapacitor.

The developed program code was embedded in the microcontroller based on Algorithm 1. The code program will configure the sensor node using the low-power mode technique to perform CO_2 measurement and send the acquired CO_2 data to the cloud of the IoT system over a Wi-Fi connection.

Algorithm 1 The logical flow of CO_2 measurement.

```
Start program while sensor node power is ON.
Initialization
Wi-Fi/internet connection.
If Wi-Fi is connected successfully:
    Start CO2 data sensing,
     CO2 data processing,
     CO2 data transmission,
    Presenting CO2 data on Adafruit dashboard,
     Logging CO2 data,
    Sleep mode until interval time is achieved.
Or Else:
    Retry Wi-Fi/internet connection.
    Return to repeat measuring data.
Stop program while sensor node power is OFF.
```

The developed sensor node characteristic is presented in Table 3.

Table 3. A basic characteristic of the wireless CO_2 sensor node.

Parameters	Value
Sensor technology	Non-Dispersive InfraRed
Sensing range	0–40,000 ppm
Sensor accuracy	±(30 ppm + 3%)
Operating voltage	3.3–5.5 V
Power storage	5.5 V 10 F supercapacitor

3.2. Graphical User Interface (GUI)

The GUI for real-time CO_2 monitoring was implemented on the Adafruit dashboard, as shown in Figure 8. The Adafruit dashboard presents the acquired CO_2 data stored in the cloud on a line graph, a gauge, and data logging. The stored data in Adafruit IO (cloud system) then can be downloaded in a spreadsheet file to be processed further.

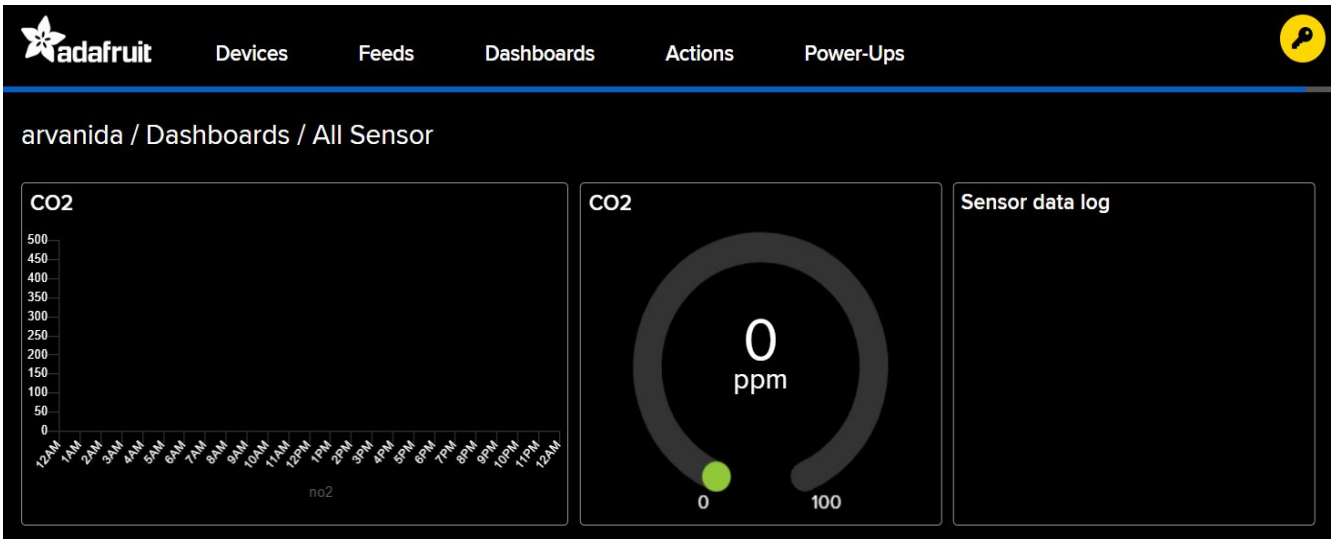

Figure 8. The dashboard monitoring.

The line graph visualizes the trend of real-time CO_2 continuously acquired data, and the gauge displays the current value of CO_2 acquired data numerically, including percentage from the maximum value of CO_2 value that is displayed graphically, and the log data display multiple lines of updated incoming and history CO_2 data from the cloud. It also displays an error message when errors happen. An alert notification can be set to provide an indication that the CO_2 concentration is higher than the threshold concentration level.

3.3. Functionality Validation Testing

This testing was performed to verify the sensor-node functionality to measure indoor CO_2 concentration data and transmit the acquired data to the cloud over the IoT system. Furthermore, the current and trend of CO_2 data can be visualized and monitored in real time on the Adafruit dashboard. The testing configuration is presented in Figure 9a. The CO_2 sensor node was connected to the monitoring terminal over a Wi-Fi/internet connection that was integrated with the IoT system.

The testing process is shown in Figure 9b. The sensor node that was already integrated with the IoT system was placed on the table inside the indoor environment. During 2 h testing periods, the sensor node continuously measured and wirelessly transmitted the CO_2 concentration data to cloud storage with a sampling rate of 1 min. At the same time, the CO_2 concentration data was visualized on the Adafruit IO dashboard on the monitoring terminal.

The testing results show that the developed sensor node has worked properly to measure indoor CO_2 concentration, send the data to the cloud over an IoT system using a Wi-Fi/internet connection, and visualize the CO_2 data on the Adafruit dashboard at the monitoring terminal. The range value of CO_2 concentration was 500–850 ppm. The CO_2 data was visualized with data history and a real-time graph using a graphical user interface, as shown in Figure 9b.

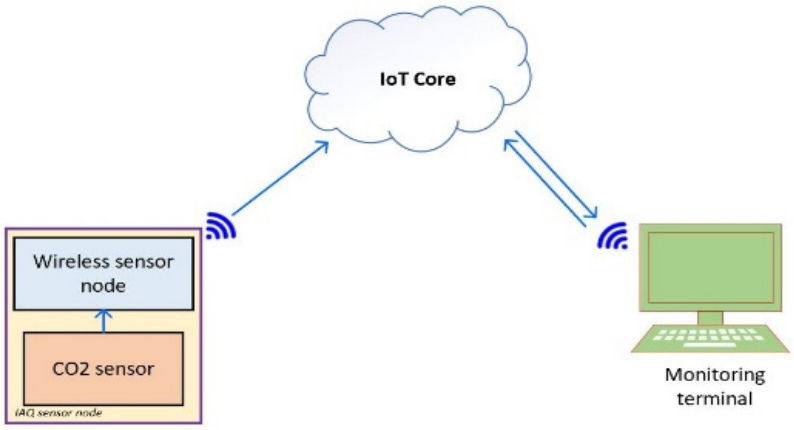

(**a**)

(**b**)

Figure 9. The CO_2 sensor node functionality testing: (**a**) configuration; (**b**) testing process and result.

3.4. Calibration

The sensor-node calibration was conducted by comparing the sensor-node measurement results with the measurement result of a reference measurement device (calibrated device). The Testo 440-Climate Measuring Instrument with CO_2 Probe was used as the reference device. It has a measurement range from 0 to 10,000 ppm with the accuracy of ± (50 ppm + 3% of m.v) (0 to 5000 ppm), ± (100 ppm + 5% of m.v) (0 to 10,000 ppm).

The calibration configuration is shown in Figure 10a. It is composed of a test chamber that includes CO_2 gas source in the gas storage, a CO_2 sensor node that is connected wirelessly to the terminal monitor using a Wi-Fi connection, and a CO_2 probe connected wirelessly to the Testo 440 using a Bluetooth connection. During the calibration process, CO_2 gas was supplied with a given concentration controlled by an electronic valve from CO_2 gas storage to the test chamber.

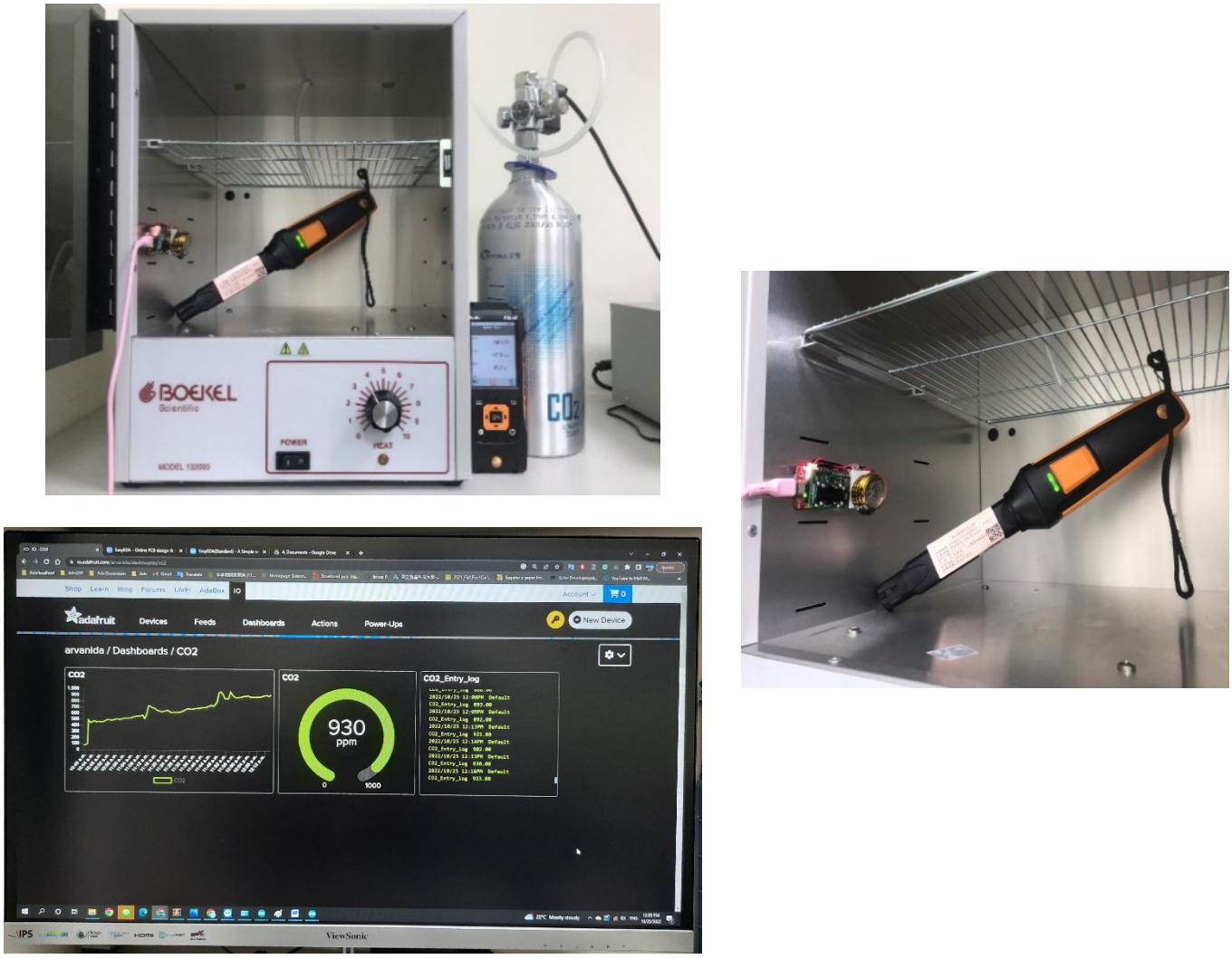

(**a**) (**b**)

Figure 10. The calibration process of sensor node: (**a**) measurement setup; (**b**) sensor node placement in a controllable test chamber.

The calibration results were carried out by CO_2 gas concentration measurement, calibration factor calculation, and validation.

3.4.1. CO_2 Concentration Measurement

The developed sensor node and CO_2 probe (validator instrument) were placed in the test chamber to measure CO_2 concentration, as shown in Figure 10b. Various CO_2 concentrations were supplied to the test chamber and measured by sensor node and CO_2 probe. The sensor node recorded the CO_2 measurement result to the terminal monitor using the Adafruit dashboard, while the CO_2 probe recorded the CO_2 measurement results to the Testo 440 terminal. The CO_2 measurement results include comparing the sensor-node and CO_2 probe readings, shown in Table 4.

Table 4. CO_2 measurement results before calibration.

Sensor Node (ppm)	Validator (ppm)	Deviation (ppm)	Absolute Percentage Deviation (%)
1751	1539	−212	13.78
1808	1597	−211	13.21
1853	1646	−207	12.58
1903	1692	−211	12.47
1949	1747	−202	11.56
2005	1804	−201	11.14
2051	1850	−201	10.86
2098	1900	−198	10.42
2152	1950	−202	10.36
2196	1999	−197	9.85
Average Deviation		−204.2	
Average Percentage Deviation			11.62

Based on the data in Table 4, the average percentage deviation of the sensor-node reading is 11.62%. The difference needs to be reduced to improve sensor-node accuracy.

3.4.2. Calibration Correction Factor Calculation

The calibration correction factor was calculated using a linear regression method to reduce the measurement result deviation between the sensor node and CO_2 probe (validator device). The calculation result is shown in Figure 11. The R^2 (coefficient of determination) value close to 1 indicates that the measurement results of the sensor node are equivalent to the measurement results of the validator device. The equation of calibration factor for CO_2 measurement by sensor node is y = 1.0336x−270.55; y is the value of CO_2 with a correction factor, and x is the CO_2 value without the correction factor. The calibration factor will include the sensor-node programming code to improve its measurement result.

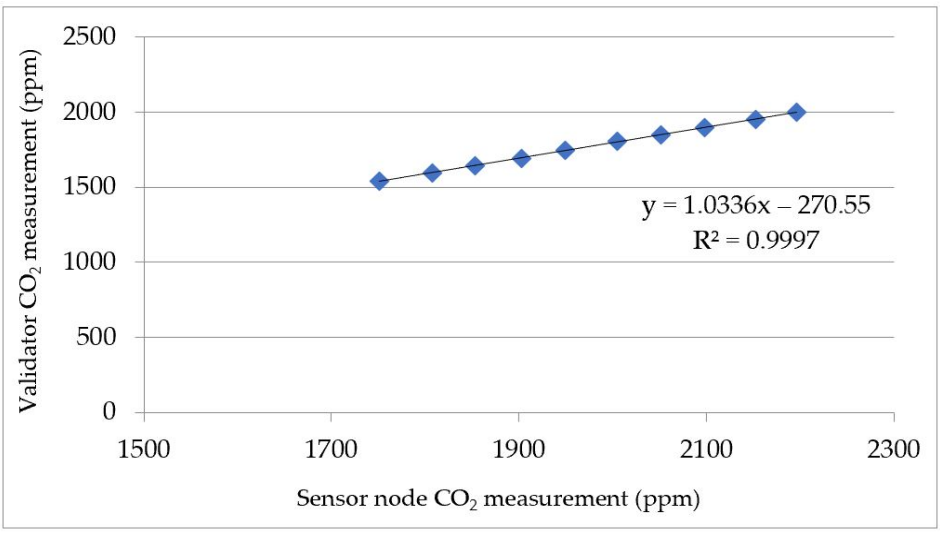

Figure 11. CO_2 compensation factor calculation.

3.4.3. Validation

The CO_2 concentration was repeatedly measured in the validation process using similar configurations and procedures, as presented in Section 3.4, in which the sensor-node programming code was updated with the calibration correction factor. Table 5 shows the measurement result and deviation between the sensor node and validator device.

Table 5. CO_2 measurement results after calibration.

Sensor Node (ppm)	Validator (ppm)	Deviation (ppm)	Absolute Percentage Deviation (%)
1514	1515	1	0.07
1600	1609	9	0.56
1650	1651	1	0.06
1705	1710	5	0.29
1743	1749	6	0.34
1812	1800	−12	0.67
1853	1855	2	0.11
1921	1899	−22	1.16
1964	1950	−14	0.72
2024	2003	−21	1.05
Average Deviation		−4.5	
Average Percentage Deviation			0.50

Based on Table 5, the average percentage deviation of measurement after calibration was 0.50%. This proved the close correlation between the developed sensor-node and reference-device measurement results.

3.5. Power Capacity Measurement

This test is necessary to obtain the power consumption of the sensor node in the one-cycle CO_2 measurement process. In the one-cycle measurement process, sensor nodes perform three processes: initialization, CO_2 sensor reading, and CO_2 data transmitting. The measurements of current consumption, time consumption, and power consumption were conducted in three processes of CO_2 measurement to obtain the sensor-node energy capacity.

3.5.1. Current Measurement

The 1NA219 power sensor was used to measure current consumption. It was coupled with the Arduino Mega to acquire the current and show the measurement result in a serial monitor using Arduino IDE. The Arduino Mega powered the 1NA219 power sensor. In contrast, the sensor node was powered by an external power supply using a micro USB cable to avoid interference between the Arduino Mega and the sensor node during the current measurement. The measurement configuration is shown in Figure 12.

The developed sensor node was set to work in two modes: active and low-power. The initialization, sensor reading, transmitting, and logging processes run in active mode with certain time intervals. The low-power mode runs in the interval between two CO_2 measurement cycles. Figure 13 shows the current consumption of sensor-node processes. The initialization process consumes a current of 42.1 mA. While in the CO_2 sensing and transmitting process, the sensor node consumes a current of 120.07 mA and 121.4 mA, respectively, the sensor node in the sleep stage consumes a current of 33.2 mA when the low-power mode is activated.

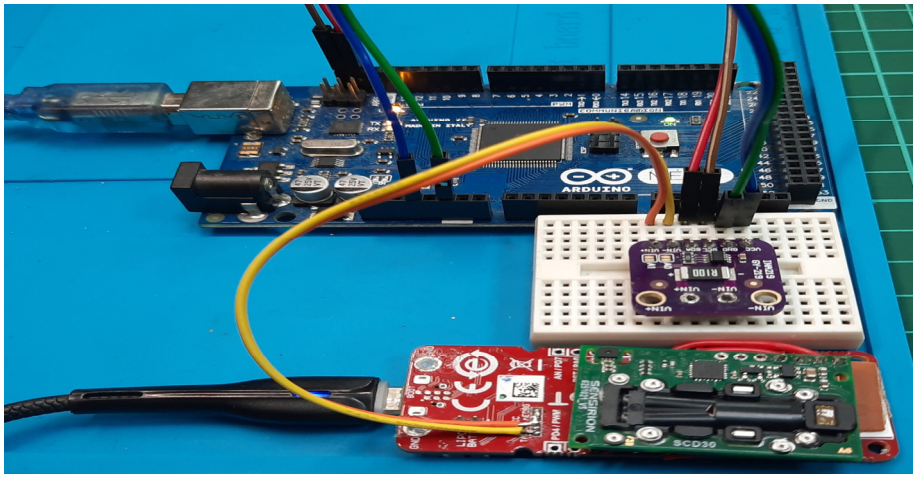

Figure 12. The current measurement configuration.

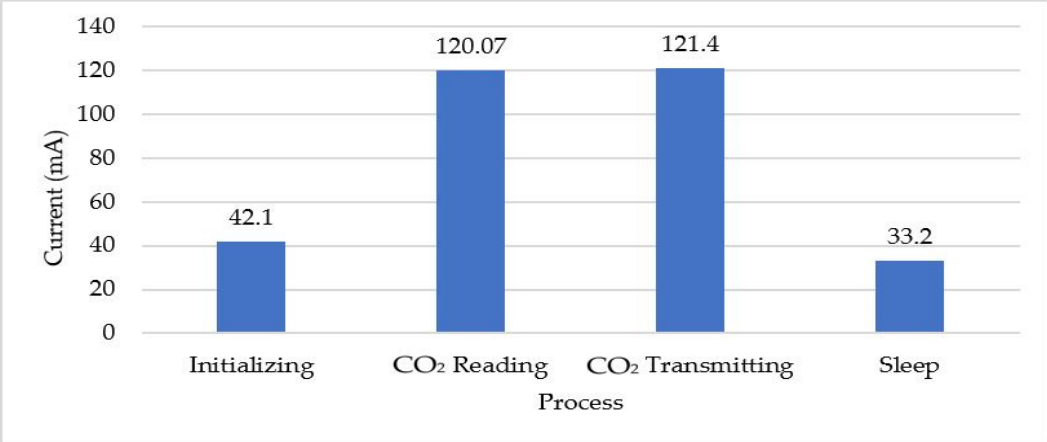

Figure 13. The current consumption of sensor-node process.

3.5.2. Time Consumption

The time measurement was conducted to obtain the time consumption of each process in CO_2 concentration measurement. Further, the time consumption was used to estimate and analyze the energy capacity of sensor nodes in one-cycle CO_2 measurement. The sensor node starts to measure CO_2 concentration with the initialization process, the CO_2 reading process, and CO_2 data-transmitting process, followed by the time interval between two CO_2 measurement cycles. A program-based measurement technique was used to measure the time consumption of each process. The program will measure the start and stop time of each process in CO_2 concentration measurement to obtain the time consumption of each process. The time-processing measurement result is shown in Figure 14. The initialization process only needs 7 ms, while the CO_2 reading and CO_2 transmitting need 25 ms and 1319 ms, respectively. The highest time consumption is in the transmitting process, depending on the internet/Wi-Fi connection. If the connection is good, the time of the transmitting process will be faster. The time consumption measurement results revealed that the total time consumption for one cycle of CO_2 measurement, including the sleep stage, is 11.351 s.

In the time interval, the sleep-mode stage can be activated, and it was set at 10 s. When this time interval scenario is applied, the sensor node runs in low-power mode operation until the time interval is achieved and returns to the initialization process to start the CO_2 measurement again. This strategy will reduce the total sensor-node energy consumption because enabling low-power mode consumes much less power than disabling low-power mode. Moreover, the time interval between two CO_2 measurement cycles (low-power mode) does not significantly affect CO_2 measurement results because of the relatively slow

change in indoor CO_2 concentration. The time interval of 10 s can still provide real-time CO_2 measurement results.

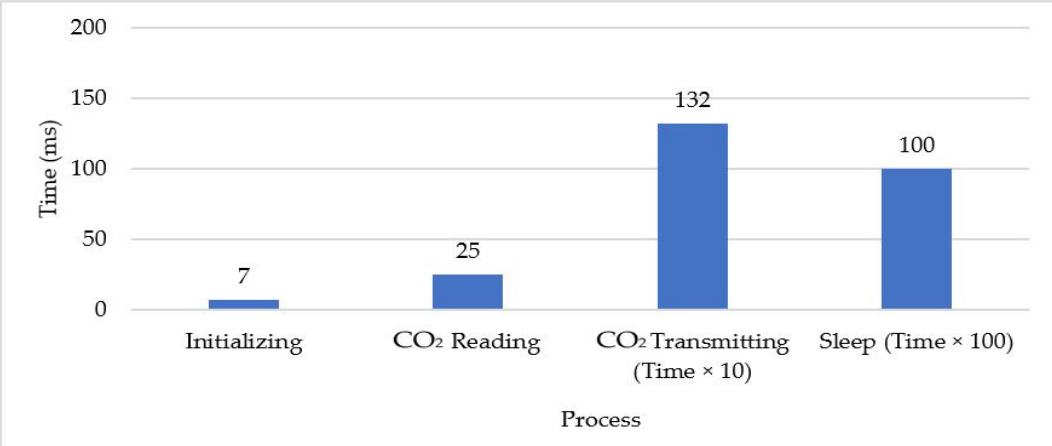

Figure 14. The time consumption of sensor node process.

3.5.3. The Energy Capacity

Sensor-node energy capacity was obtained according to the sensor node's power-consumption calculation and time-consumption measurement data. The energy capacity was calculated in one-cycle sensor-node operation with the interval between cycles set to 10 s. The sensor-node energy capacity is presented in Table 6. The sensor node consumes the highest power of 392.12 mW in CO_2 transmitting process and the lowest power of 106.90 mW in the sensor-node sleep stage. However, the highest energy capacity sensor node is in the sleep stage, which requires 0.2970 mWh (66.94%), as described in Figure 15. This is because the sleep stage was set with the longest duration among other processes, with a duration of 10 s. From Table 6, the total energy capacity of the sensor node is 0.4436 mWh for one-cycle sensor-node operation, including measurement time interval. These results indicate that a supercapacitor has the potential to be used as power storage for energy harvester in further study.

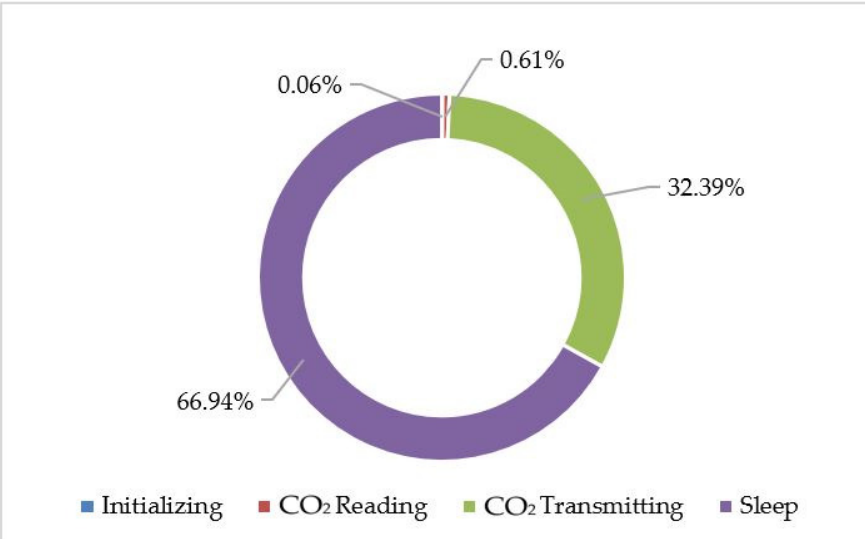

Figure 15. The percentage of energy capacity requirement.

Table 6. Energy capacity.

Process	Voltage (V)	Current (mA)	Power (mW)	Time (ms)	Energy Capacity Required (mWh)
Initializing	3.22	42.1	135.56	7	0.0003
CO_2 Reading	3.22	120.07	387.83	25	0.0027
CO_2 Transmitting	3.22	121.4	392.12	1319.33	0.1437
Sleep	3.22	33.2	106.9	10,000	0.297
Total Energy Required (one cycle)					0.4436

3.5.4. Power Storage Testing

This test was conducted for a series of 2 unit 5.5 V 5.0 F supercapacitors equipped on the sensor node. The test examined the charge and discharge time of the supercapacitor is one cycle of CO_2 measurement. The energy capacity required by the sensor node in one cycle of CO_2 measurement was 0.4436 mWh.

The charging time was obtained at 111 s to achieve the voltage of 4.37 V from 3.57 V, and the discharging time was obtained at 108 s from the voltage of 3.64 V to 3.11 V. Therefore, the power storage can be used well. The result is shown in Figure 16.

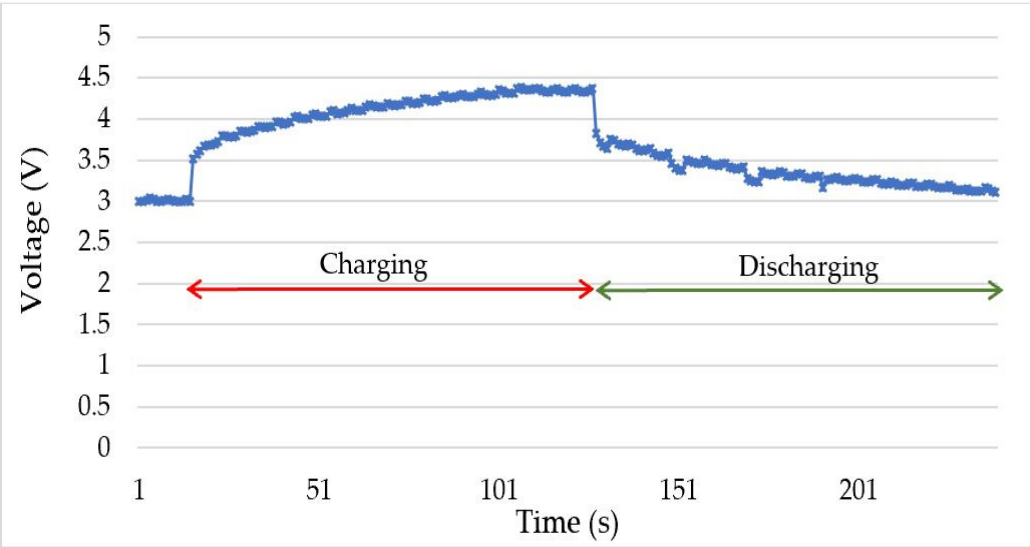

Figure 16. Power storage charging and discharging voltage.

3.6. CO_2 Concentration Measurement Experiment

3.6.1. Configuration

The field experiment was conducted to examine the performance of the developed sensor node in acquiring CO_2 concentration. The experimental configuration is shown in Figure 17. The developed sensor node was used to measure indoor CO_2 data sent to the Adafruit dashboard in the monitor terminal over the IoT system. In the terminal monitor, the CO_2 data be visualized in the real-time and continuous graph, current numeric data, and updated logging data.

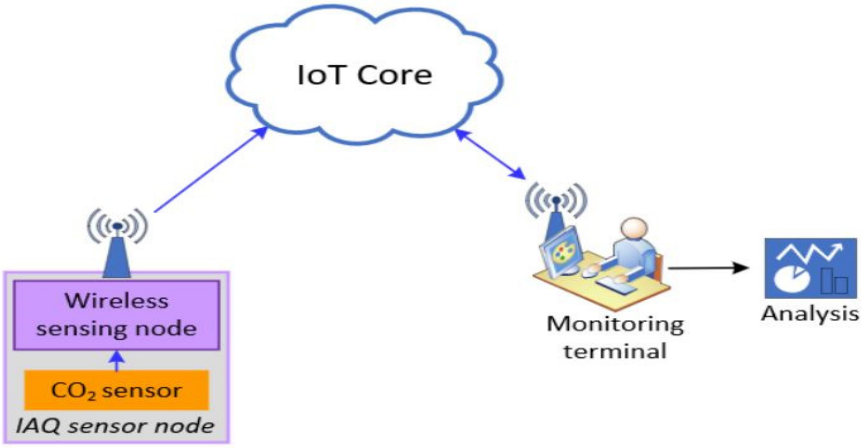

Figure 17. CO_2 sensor node configuration for the field experiment.

The measurement targets were the CO_2 concentration of an indoor laboratory and outdoor environment. The entire laboratory comprises laboratory equipment, three students, computers, and furniture with a room dimension of 6.0 m × 3.5 m. The outdoor environment was around the student dormitory. The field experiment for indoor measurement was conducted in three and a half days from 19 May to 22 May 2022, and outdoor measurement was conducted in three and a half days from 25 May to 27 May 2022

3.6.2. Measurement Result

During the field experiment, the sensor node worked properly by acquiring indoor CO_2 concentration and transferring the data to the cloud over the IoT system to be visualized on the Adafruit dashboard, as shown in Figure 18a for the measurement in an indoor room and Figure 18b for outdoor.

The trend of CO_2 recorded data was presented in a spreadsheet chart shown in Figure 19 that can be used for further analysis. The field experiment result shows that the sensor node can monitor and record indoor CO_2 concentration levels in real time and continuously within ranges of 286 ppm to 670 ppm, and outdoors in ranges of 129 ppm to 997 ppm. The average CO_2 concentration level measurement in an indoor room is 314 ppm, while the average CO_2 concentration level measurement outdoors is 423 ppm. These results indicate that the outdoor CO_2 concentration level is higher than the indoor concentration level. The total of people in the room, the people's activity, and the ventilation condition contribute to the high indoor CO_2 concentration.

The field experiment results revealed that the sensor node provides accurate measurement results in different environmental conditions (indoor and outdoor) with various and fluctuating CO_2 concentrations.

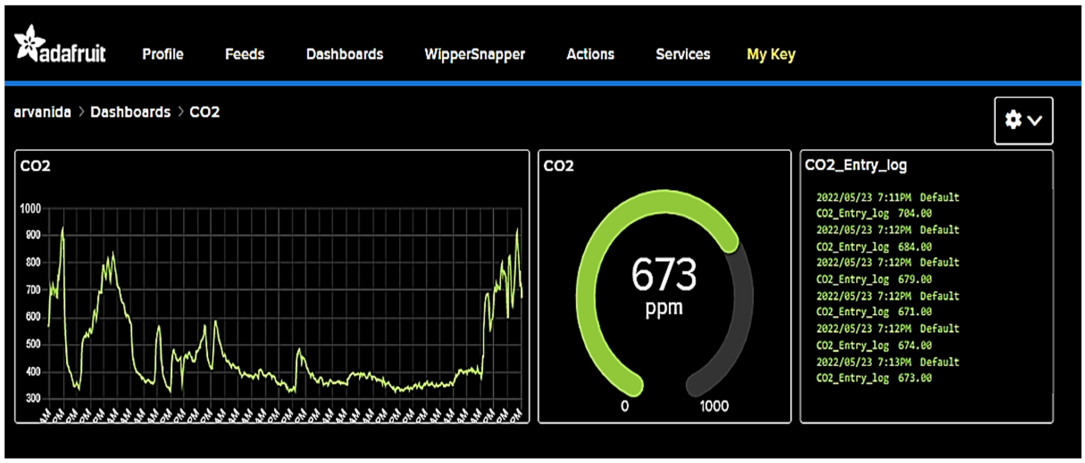

(**a**)

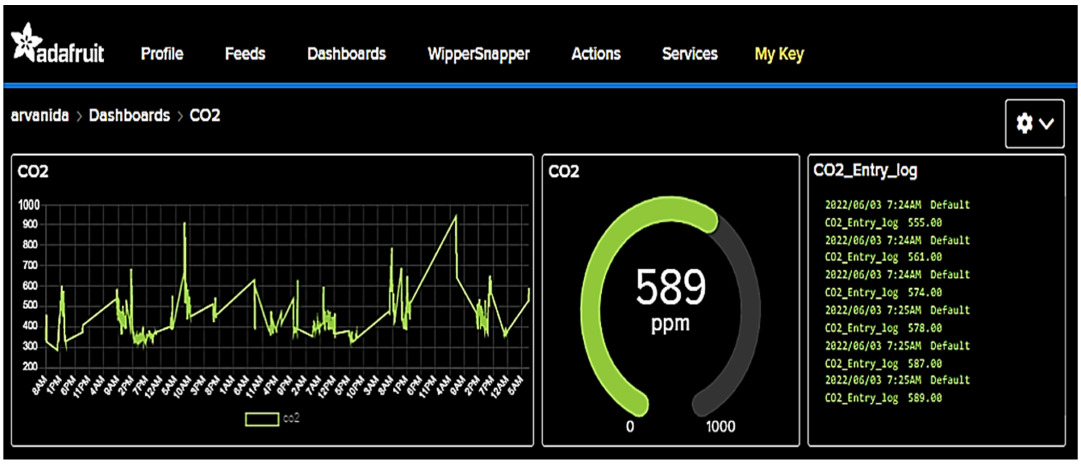

(**b**)

Figure 18. Visualization of CO_2 measurement on a dashboard: (**a**) indoor environment; (**b**) outdoor environment.

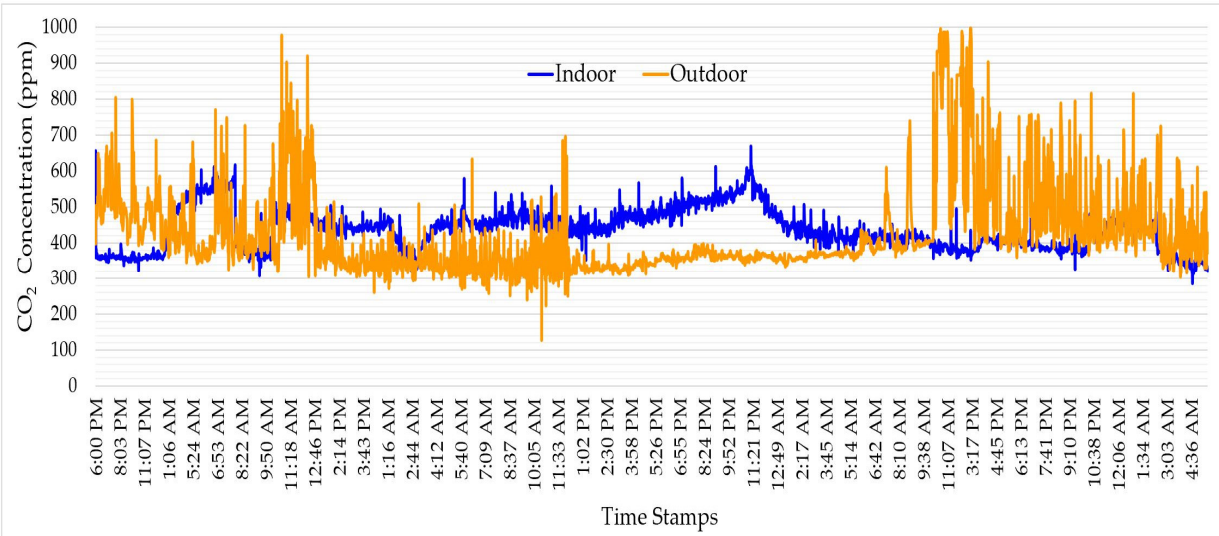

Figure 19. The CO_2 concentration trend in the field experiment.

4. Conclusions

The smart wireless CO_2 sensor-node prototype was implemented in a compact size on a single board with a dimension of 25 mm x 60 mm. The node was built using low-cost and low-power components available in the market. The functionality and performance test shows that the developed sensor node consumes quick time and low energy for one cycle of CO_2 measurement (initialization, data acquired, data transmitted, sleep mode). It consumes only 11.351 s and 0.4436 mWh, respectively, to provide real-time and continuous indoor CO_2 concentration data with a time interval of 10 s. With this energy consumption, the main power storage (supercapacitor) can power the sensor node in 108 s. However, the capacity of the supercapacitor can be increased to extend the sensor-node life. Another potential method is integrating the sensor node with a micro energy harvester to harvest energy from indoor ambient energy sources (artificial light, ambient temperature, airflow rate) in further development. It considers building an autonomous sensor node for long periods of indoor CO_2 monitoring applications with an energy generator to extend the sensor node life.

The validation and field experiment results show that the developed sensor node has high accuracy with a measurement error of 0.5% and provides real-time, continuous, and remote measurement of CO_2 concentrations in indoor and outdoor environments. This proved that the measurements were easily accessed using an IoT system on a graphical user interface.

The measurement results and features of the developed sensor node are very promising and suitable for indoor air-quality monitoring applications, indicating that the sensor node could be applied for long periods of monitoring and recording indoor CO_2 concentration data. Thus, the indoor CO_2 concentration measurement data can be utilized as an indicator to minimize the risk of the indoor SARS-CoV-2 airborne transmission.

Author Contributions: Conceptualization, C.B.D.K.; methodology, C.B.D.K. and A.A.; formal analysis, A.A. and A.F.P.; investigation, A.A. and A.F.P.; supervision, C.B.D.K.; resources, C.B.D.K.; writing—original draft preparation, A.A. and A.F.P.; writing—review and editing, C.B.D.K. All authors have read and agreed to the published version of the manuscript.

Funding: This research funding was by the Ministry of Science and Technology of Taiwan (MOST: 110-2222-E-167-003-MY3).

Data Availability Statement: The data presented in this study are available at the request of the corresponding author.

Acknowledgments: The authors would like to thank the Ministry of Science and Technology of Taiwan for funding support and the Refrigeration, Air Conditioning, and Energy Engineering Department of the National Chin-Yi University of Technology, Taiwan, for support in the system design.

Conflicts of Interest: The authors declare no conflict of interest.

References

1. Seguel, J.M.; Merrill, R.; Seguel, D.; Campagna, A.C. Indoor Air Quality. *Am. J. Lifestyle Med.* **2017**, *11*, 284–295. [CrossRef] [PubMed]
2. Ana, G.R.; Alli, A.S.; Uhiara, D.C.; Shendell, D.G. Indoor Air Quality and Reported Health Symptoms among Hair Dressers in Salons in Ibadan, Nigeria. *J. Chem. Health Saf.* **2019**, *26*, 23–30. [CrossRef]
3. Theodosiou, T.G.; Ordoumpozanis, K.T. Energy, Comfort and Indoor Air Quality in Nursery and Elementary School Buildings in the Cold Climatic Zone of Greece. *Energy Build.* **2008**, *40*, 2207–2214. [CrossRef]
4. Jafari, M.J.; Khajevandi, A.A.; Mousavi Najarkola, S.A.; Yekaninejad, M.S.; Pourhoseingholi, M.A.; Omidi, L.; Kalantary, S. Association of Sick Building Syndrome with Indoor Air Parameters. *Tanaffos* **2015**, *14*, 55–62. [PubMed]
5. Pitarma, R.; Marques, G.; Ferreira, B.R. Monitoring Indoor Air Quality for Enhanced Occupational Health. *J. Med. Syst.* **2017**, *41*, 23. [CrossRef]
6. Becerra, J.A.; Lizana, J.; Gil, M.; Barrios-Padura, A.; Blondeau, P.; Chacartegui, R. Identification of Potential Indoor Air Pollutants in Schools. *J. Clean. Prod.* **2020**, *242*, 118420. [CrossRef]
7. Lee, S.C.; Chang, M. Indoor and Outdoor Air Quality Investigation at Schools in Hong Kong. *Chemosphere* **2000**, *41*, 109–113. [CrossRef]

8. Branco, P.T.B.S.; Alvim-Ferraz, M.C.M.; Martins, F.G.; Sousa, S.I.V. Children's Exposure to Indoor Air in Urban Nurseries-Part I: CO_2 and Comfort Assessment. *Environ. Res.* **2015**, *140*, 1–9. [CrossRef]
9. World Health Organization. *International Labour Organization Preventing and Mitigating COVID-19 at Work: Policy Brief, 19 May 2021*; World Health Organization: Geneva, Switzerland, 2021.
10. Wang, W.; Wang, J.; Chen, J.; Huang, G.; Guo, X. Multi-Zone Outdoor Air Coordination through Wi-Fi Probe-Based Occupancy Sensing. *Energy Build.* **2018**, *159*, 495–507. [CrossRef]
11. Peng, Z.; Jimenez, J.L. Exhaled CO_2 as a COVID-19 Infection Risk Proxy for Different Indoor Environments and Activities. *Environ. Sci. Technol. Lett.* **2021**, *8*, 392–397. [CrossRef]
12. Rudnick, S.N.; Milton, D.K. Risk of Indoor Airborne Infection Transmission Estimated from Carbon Dioxide Concentration. *Indoor Air* **2003**, *13*, 237–245. [CrossRef] [PubMed]
13. Bazant, M.Z.; Kodio, O.; Cohen, A.E.; Khan, K.; Gu, Z.; Bush, J.W.M. Monitoring Carbon Dioxide to Quantify the Risk of Indoor Airborne Transmission of COVID-19. *Flow* **2021**, *1*, E10. [CrossRef]
14. Barbieri, P.; Zupin, L.; Licen, S.; Torboli, V.; Semeraro, S.; Cozzutto, S.; Palmisani, J.; Di Gilio, A.; de Gennaro, G.; Fontana, F.; et al. Molecular Detection of SARS-CoV-2 from Indoor Air Samples in Environmental Monitoring Needs Adequate Temporal Coverage and Infectivity Assessment. *Environ. Res.* **2021**, *198*, 111200. [CrossRef] [PubMed]
15. Buonanno, G.; Morawska, L.; Stabile, L. Quantitative Assessment of the Risk of Airborne Transmission of SARS-CoV-2 Infection: Prospective and Retrospective Applications. *Environ. Int.* **2020**, *145*, 106112. [CrossRef]
16. Miller, S.L.; Nazaroff, W.W.; Jimenez, J.L.; Boerstra, A.; Buonanno, G.; Dancer, S.J.; Kurnitski, J.; Marr, L.C.; Morawska, L.; Noakes, C. Transmission of SARS-CoV-2 by Inhalation of Respiratory Aerosol in the Skagit Valley Chorale Superspreading Event. *Indoor Air* **2021**, *31*, 314–323. [CrossRef]
17. Morawska, L.; Milton, D.K. It Is Time to Address Airborne Transmission of Coronavirus Disease 2019 (COVID-19). *Clin. Infect. Dis.* **2020**, *71*, 2311–2313. [CrossRef]
18. Bhagat, R.K.; Davies Wykes, M.S.; Dalziel, S.B.; Linden, P.F. Effects of Ventilation on the Indoor Spread of COVID-19. *J. Fluid Mech.* **2020**, *903*, F1. [CrossRef]
19. Zivelonghi, A.; Lai, M. Mitigating Aerosol Infection Risk in School Buildings: The Role of Natural Ventilation, Volume, Occupancy and CO_2 Monitoring. *Build. Environ.* **2021**, *204*, 108139. [CrossRef]
20. Tang, S.; Mao, Y.; Jones, R.M.; Tan, Q.; Ji, J.S.; Li, N.; Shen, J.; Lv, Y.; Pan, L.; Ding, P.; et al. Aerosol Transmission of SARS-CoV-2? Evidence, Prevention and Control. *Environ. Int.* **2020**, *144*, 106039. [CrossRef]
21. van Doremalen, N.; Bushmaker, T.; Morris, D.H.; Holbrook, M.G.; Gamble, A.; Williamson, B.N.; Tamin, A.; Harcourt, J.L.; Thornburg, N.J.; Gerber, S.I.; et al. Aerosol and Surface Stability of SARS-CoV-2 as Compared with SARS-CoV-1. *N Engl J Med* **2020**, *382*, 1564–1567. [CrossRef]
22. Riley, E.C.; Murphy, G.; Riley, R.L. Airborne Spread of Measles in a Suburban Elementary School. *Am. J. Epidemiol.* **1978**, *107*, 421–432. [CrossRef] [PubMed]
23. Kwon, J.; Ahn, G.; Kim, G.; Kim, J.C.; Kim, H. A Study on NDIR-Based CO_2 Sensor to Apply Remote Air Quality Monitoring System. In Proceedings of the 2009 ICCAS-SICE, Fukuoka, Japan, 18–21 August 2009; pp. 1683–1687.
24. Scislo, L.; Szczepanik-Scislo, N. Air Quality Sensor Data Collection and Analytics With IoT for an Apartment With Mechanical Ventilation. In Proceedings of the 2021 11th IEEE International Conference on Intelligent Data Acquisition and Advanced Computing Systems: Technology and Applications (IDAACS), Cracow, Poland, 22–25 September 2021; IEEE: Cracow, Poland, 2021; pp. 932–936.
25. Abraham, S.; Li, X. Design of A Low-Cost Wireless Indoor Air Quality Sensor Network System. *Int. J. Wirel. Inf. Netw.* **2016**, *23*, 57–65. [CrossRef]
26. Kanál, A.K.; Tamás, K. Assessment of Indoor Air Quality of Educational Facilities Using an IoT Solution for a Healthy Learning Environment. In Proceedings of the 2020 IEEE International Instrumentation and Measurement Technology Conference (I2MTC), Dubrovnik, Croatia, 25–28 May 2020; pp. 1–6.
27. Ortiz Perez, A.; Bierer, B.; Scholz, L.; Wöllenstein, J.; Palzer, S. A Wireless Gas Sensor Network to Monitor Indoor Environmental Quality in Schools. *Sensors* **2018**, *18*, 4345. [CrossRef] [PubMed]
28. Wisesa, H. CO_2 Monitoring System Prototype Using Wireless Sensor Network. *Int. J. Inf. Commun. Technol. (IJoICT)* **2017**, *2*, 49. [CrossRef]
29. Muladi, M.; Sendari, S.; Widiyaningtyas, T. Real Time Indoor Air Quality Monitoring Using Internet of Things at University. In Proceedings of the 2018 2nd Borneo International Conference on Applied Mathematics and Engineering (BICAME), Balikpapan, Indonesia, 10–11 December 2018; pp. 169–173.
30. Rucsandoiu, M.L.; Antonescu, A.M.; Enachescu, M. Indoor Air Quality Monitoring Platform. In Proceedings of the 2021 International Symposium on Signals, Circuits and Systems (ISSCS), Iasi, Romania, 15–16 July 2021; pp. 1–4.
31. Dai, X.; Liu, J.; Li, X.; Zhao, L. Long-Term Monitoring of Indoor CO_2 and PM2.5 in Chinese Homes: Concentrations and Their Relationships with Outdoor Environments. *Build. Environ.* **2018**, *144*, 238–247. [CrossRef]
32. Palmisani, J.; Di Gilio, A.; Viana, M.; de Gennaro, G.; Ferro, A. Indoor Air Quality Evaluation in Oncology Units at Two European Hospitals: Low-Cost Sensors for TVOCs, PM2.5 and CO_2 Real-Time Monitoring. *Build. Environ.* **2021**, *205*, 108237. [CrossRef]
33. Yin, H.; Zhai, X.; Ning, Y.; Li, Z.; Ma, Z.; Wang, X.; Li, A. Online Monitoring of PM2.5 and CO_2 in Residential Buildings under Different Ventilation Modes in Xi'an City. *Build. Environ.* **2022**, *207*, 108453. [CrossRef]

34. Fernández-Ramos, M.D.; Moreno-Puche, F.; Escobedo, P.; García-López, P.A.; Capitán-Vallvey, L.F.; Martínez-Olmos, A. Optical Portable Instrument for the Determination of CO_2 in Indoor Environments. *Talanta* **2020**, *208*, 120387. [CrossRef]
35. Canada, H. Consultation: Proposed Residential Indoor Air Quality Guidelines for Carbon Dioxide. Available online: https://www.canada.ca/en/health-canada/programs/consultation-residential-indoor-air-quality-guidelines-carbon-dioxide/document.html (accessed on 4 June 2022).
36. Pietrucha, T. Ability to Determine the Quality of Indoor Air in Classrooms without Sensors. *E3S Web Conf.* **2017**, *17*, 73. [CrossRef]
37. Vanzo, T. The Dangers of High Carbon Dioxide (CO2) Levels. *Smart Air* **2021**. Available online: https://smartairfilters.com/en/blog/dangers-high-carbon-dioxide-co2-levels/ (accessed on 20 June 2022).
38. CDC Coronavirus Disease 2019 (COVID-19). Available online: https://www.cdc.gov/coronavirus/2019-ncov/more/science-and-research/surface-transmission.html (accessed on 23 May 2022).
39. Meyerowitz, E.A.; Richterman, A.; Gandhi, R.T.; Sax, P.E. Transmission of SARS-CoV-2: A Review of Viral, Host, and Environmental Factors. *Ann. Intern. Med.* **2021**, *174*, 69–79. [CrossRef] [PubMed]
40. Kampf, G.; Brüggemann, Y.; Kaba, H.E.J.; Steinmann, J.; Pfaender, S.; Scheithauer, S.; Steinmann, E. Potential Sources, Modes of Transmission and Effectiveness of Prevention Measures against SARS-CoV-2. *J. Hosp. Infect.* **2020**, *106*, 678–697. [CrossRef] [PubMed]
41. Curtius, J.; Granzin, M.; Schrod, J. Testing Mobile Air Purifiers in a School Classroom: Reducing the Airborne Transmission Risk for SARS-CoV-2. *Aerosol Sci. Technol.* **2021**, *55*, 586–599. [CrossRef]
42. Drossinos, Y.; Stilianakis, N.I. What Aerosol Physics Tells Us about Airborne Pathogen Transmission. *Aerosol Sci. Technol.* **2020**, *54*, 639–643. [CrossRef]
43. ATMEGA4808 | Microchip Technology. Available online: https://www.microchip.com/en-us/product/ATMEGA4808# (accessed on 11 May 2022).
44. ATmega4808/4809 Data Sheet. Available online: https://onlinedocs.microchip.com/pr/GUID-4E9DA219-611B-4772-B5D3-9ED908198864-en-US-16/index.html?GUID-0E8898B7-7398-4EBA-A96F-7E9353ECE5E4 (accessed on 11 May 2022).
45. Yi, S.; Park, Y.; Han, S.; Min, N.; Kim, E.; Ahn, T. Novel NDIR CO/Sub 2/ Sensor for Indoor Air Quality Monitoring. In Proceedings of the 13th International Conference on Solid-State Sensors, Actuators and Microsystems, 2005. Digest of Technical Papers, Seoul, Korea, 5–9 June 2005; IEEE: Seoul, Korea, 2005; Volume 2, pp. 1211–1214.
46. SCD30-CO_2 accuracy of ±(30 Ppm + 3% MV) @400-10000 Ppm. Available online: https://sensirion.com/products/catalog/SCD30/ (accessed on 13 May 2022).
47. ATWINC1510-IC | Microchip Technology. Available online: https://www.microchip.com/en-us/product/ATWINC1510-IC (accessed on 13 May 2022).
48. Kuncoro, C.B.D.; Permana, A.F.; Asyikin, M.B.Z.; Adristi, C. Smart Wireless Climate Sensor Node for Indoor Comfort Quality Monitoring Application. *Energies* **2022**, *15*, 2939. [CrossRef]